

Beyond Multiple Instance Learning: Full Resolution All-In-Memory End-To-End Pathology Slide Modeling

Gabriele Campanella^{1,2}, Eugene Fluder³, Jennifer Zeng⁴, Chad Vanderbilt⁵, Thomas J. Fuchs^{1,2}

1. Windreich Department of Artificial Intelligence and Human Health, Icahn School of Medicine at Mount Sinai, New York
2. Hasso Plattner Institute for Digital Health at Mount Sinai, Icahn School of Medicine at Mount Sinai, New York
3. Scientific Computing and Data, Icahn School of Medicine at Mount Sinai, New York
4. Department of Pathology, Molecular and Cell-Based Medicine, Icahn School of Medicine at Mount Sinai, New York
5. Department of Pathology, Memorial Sloan Kettering Cancer Center, New York

Abstract

Artificial Intelligence (AI) has great potential to improve health outcomes by training systems on vast digitized clinical datasets. Computational Pathology, with its massive amounts of microscopy image data and impact on diagnostics and biomarkers, is at the forefront of this development. Gigapixel pathology slides pose a unique challenge due to their enormous size and are usually divided into tens of thousands of smaller tiles for analysis. This results in a discontinuity in the machine learning process by separating the training of tile-level encoders from slide-level aggregators and the need to adopt weakly supervised learning strategies. Training models from entire pathology slides end-to-end has been largely unexplored due to its computational challenges. To overcome this problem, we propose a novel approach to jointly train both a tile encoder and a slide-aggregator fully in memory and end-to-end at high-resolution, bridging the gap between input and slide-level supervision. While more computationally expensive, detailed quantitative validation shows promise for large-scale pre-training of pathology foundation models.

Introduction

The application of Artificial Intelligence (AI) in the medical domain has the potential to improve health and disease outcomes of the population at large. The advent of AI in healthcare is driven by the digitization of vast quantities of clinical data. In recent years, pathology departments around the world have started transitioning to a digital workflow which includes scanning pathology slides, paving the way for the emergence of computational pathology and the development of AI-based systems for diagnosis and prognosis in pathology. Compared to other medical image modalities, like radiology, digitized pathology slides are orders of magnitude larger resulting in giga-pixel images that can span over 100,000 pixels in each dimension at 40x magnification. Processing these very large images is challenging, leading to the common strategy in pathology to divide slides into tens of thousands of small tiles for analysis.

Weakly supervised learning is often used, frequently formalized with multiple instance learning (MIL)¹, to train predictive models.

To this date, most works in computational pathology fall into two main categories: approaches that focus on training a tile-level encoder, and approaches that focus on training a slide-level aggregator commonly leveraging a pre-trained encoder for feature extraction. Tile-level encoders can be trained to directly extract relevant features for specific tasks. An example is Campanella et al.² where a clinical-grade decision support system was trained on a large scale using max-pool MIL. In contrast, aggregator strategies rely on extracting features from tiles using a frozen encoder which has been previously trained on a different task^{3,4}. This is because training an encoder and aggregator end-to-end is too memory intensive for a single GPU. Originally, ImageNet pre-trained encoders were used for this purpose. More recently, with the success of self-supervised learning (SSL) for large-scale pretraining of visual encoders, pre-trained models on pathology data have been published⁵⁻¹¹ and a transition from ImageNet based encoders to pathology tailored ones is occurring. While SSL strategies applied to pathology can achieve better performance in various downstream tasks compared to ImageNet trained models¹¹, it is still unknown whether current SSL strategies result in encoders that show optimal downstream task performance.

Due to the aforementioned challenges, not much attention has been given to the idea of training models from an entire pathology slide in an end-to-end fashion. Xie et al.¹² presented a method that allows to train an encoder directly from slide labels by clustering the feature space and representing a slide as a list of tiles closest in feature space to learned prototypes. In Qu et al.¹³, they proposed to train in a slide aggregator and tile encoder by using the attention scores of the aggregator to guide tile selection for training the encoder. In general, for all these methods there is no gradient directly connecting the aggregator and encoder parts of the model that can leverage the entire slide at once. To the best of our knowledge, the only comparable work was published in 2023 by Wang et al.¹⁴ where they applied LongNet¹⁵, a self-attention algorithm with linear scaling memory, to computational pathology. While they train a ViT from image pixels over an entire slide, their pipeline relies on drastically down sampling the slide resolution, potentially losing cellular level information which may be important for certain tasks.

In contrast to all previous work, we propose to learn both a tile encoder and a slide-aggregator fully in memory and end-to-end at high-resolution, where the slide-level loss backpropagates directly through the aggregator and tile encoder. We achieve this via GPU-parallelization and customized GPU-GPU communication. We apply this framework to a clinically relevant task in cancer research for which we have thoroughly investigated other training strategies, including fully supervised and weakly supervised strategies, tile-level and slide-level algorithms, as well as the use of large scale self-supervised learning pre-training. We show the value of the proposed framework when compared to current computational pathology approaches. Since our framework is more computationally expensive compared to other popular algorithms, we argue that its best use will be in large-scale pre-training of pathology foundation models.

Method

Modern GPUs allow to jointly train a tile encoder and slide aggregator end-to-end by subsampling K tiles from each slide so that in each optimization step a single slide is considered. This can be considered

an extension of MIL where from the original bags K -sized pseudo-bags are sampled instead. This simple strategy can be improved by choosing which tiles to sample based on more complex criteria. This is similar to the work in Xie et al.¹², where a memory bank of cluster centroids is used to select a set of heterogeneous tile from each slide. In Figure 1 we show the memory requirements of this strategy using various popular vision architectures including convolutional neural networks (Figure 1a) and vision transformers (Figure 1b) for the encoder network. For these experiments we generate a dummy loss from the features extracted by the encoder without the use of a slide aggregator. We show that on an H100 GPU with 80GB of RAM, it is possible to run forward and backward passes with at most 840 tiles for a ResNet50, and 528 tiles for a ViT-base model. We can further boost K , and increase processing speeds, by using mixed precision techniques such as automatic mixed precision (AMP). Using AMP with automatic casting to 16-bit float precision it is possible to analyze 1,848 and 728 tiles for a ResNet50 and a ViT-base respectively.

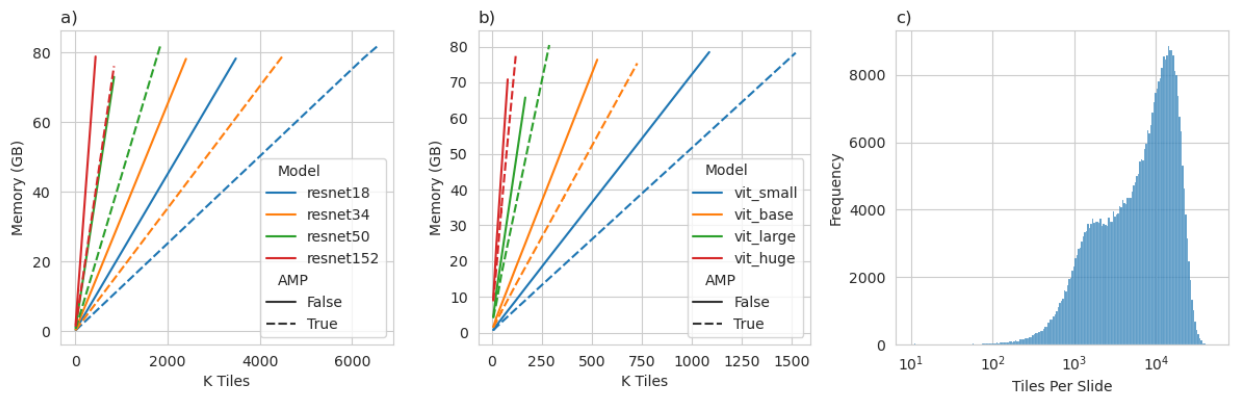


Figure 1. a) H100 GPU memory usage for training ResNet encoders of different sizes. b) H100 GPU memory usage for training ViT encoders of different sizes. Full precision and AMP training are compared. c) Distribution of 20x magnification non-overlapping tissue tiles per slide in a large health system-level dataset.

It is possible to parallelize feature encoding by assigning K tiles to N GPUs to encode NK tiles. Whole slide images can contain tens of thousands and potentially even hundreds of thousands of tiles. In Figure 1c we show the distribution of non-overlapping tissue tiles per slide of size 256 pixels extracted at 20x magnification (0.5 MPP) for the pre-training dataset described in Campanella et al.¹¹. This dataset encompasses pathology data at a health-system scale and can be considered a good representation of clinical pathology slides in general. In this dataset, the highest number of tiles in a slide is 50,578 where 99% of slides contain less than 27,219 tiles and 90% of slides contain less than 18,766. With a ViT-base using AMP is possible to encode a full slide using 70, 38, and 26 H100 GPUs respectively. It is important to note that while 20x magnification is the most commonly used resolution, for certain applications where cellular and nuclear features are important, it may be necessary to use 40x magnification which will increase by a factor of 4 the number of tiles per slide.

Next, we discuss how to allow training of an encoder and aggregator end-to-end using the encoder parallelism described above. We propose to separate encoding and aggregation to different GPU groups, where these groups can consist of multiple GPUs. In practice, the encoding group consists of multiple GPUs, while the aggregator group can consist of only one GPU. This is consistent with the fact that the vast majority of current aggregation strategies rely on a single GPU. To allow for training we customize GPU-GPU communications to simulate the flow of activations and gradients as if the data was

processed on a single GPU card. Assuming a GPU cluster with $N + 1$ GPUs, we denote rank 0 as the aggregator process and ranks $1, \dots, N$ the encoder processes. For each epoch and slide, a distributed sampler directs the N batches of images to the N GPUs while rank 0 waits for input. Next, the encoder processes perform a forward pass through the encoder to generate features. At this stage, feature vectors from ranks $1, \dots, N$ are sent to rank 0 via a gather call. The gather call breaks the computing graph and we will have to route the gradients manually during the backward pass. Rank 0 then concatenates these into a single feature matrix that is the input to the aggregation model which generates a slide level feature vector that is projected to class logits or other output for loss computation. During the backward phase, aggregator gradients are generated from the loss l in rank 0 back to the input features. The feature gradients are then split into N chunks and sent to each respective rank via a scatter call. To propagate the gradients back to the encoder model, each process with rank $1, \dots, N$ generates a pseudo-loss l_e based on the features output from the encoder f and the feature gradient g coming from rank 0:

$$l_e = N \sum_{i=1}^F f_i g_i$$

To note that the pseudo-loss must be scaled by the number of processes in the encoder group N to recover the expected gradient magnitude. We leverage torch's DistributedDataParallel¹⁶ (DDP) to wrap the encoder model which automatically ensures that gradients will be all-reduced and the models' weights are the same after optimization across all ranks $1, \dots, N$. Figure 2 summarizes the method.

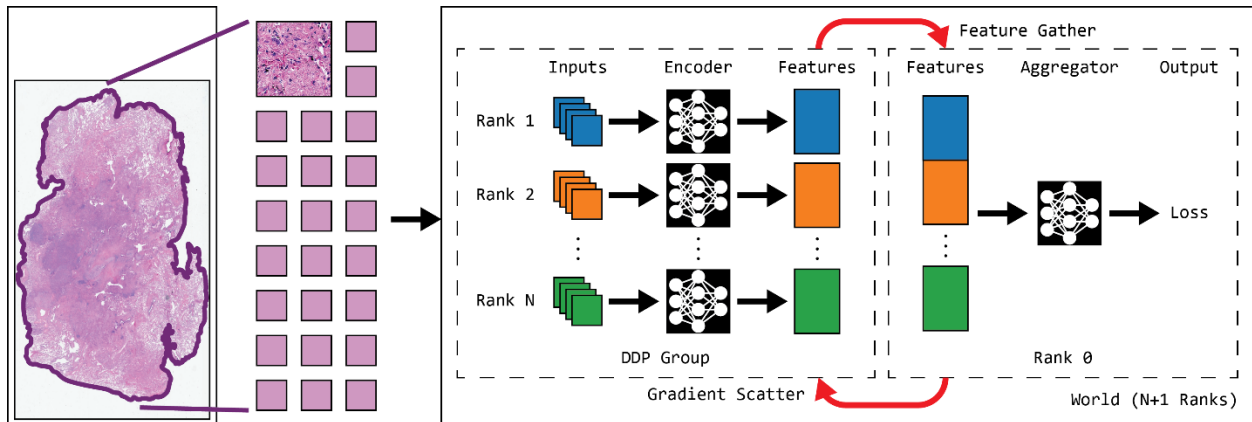


Figure 2. Overview of the proposed method. Tissue tiles from slides are extracted. A distributed sampler generates appropriate batches to each encoder rank in the DDP group. Features generated by the encoder ranks are gathered and concatenated in rank 0. Aggregator forward and backward passes are executed in rank 0. The gradients of the input features to the aggregator are split and scattered to the appropriate rank. In each rank a pseudo-loss is generated to use torch's automatic differentiation. Since the encoder models are wrapped in DDP, models are synchronized across ranks after optimization.

One advantage of the proposed framework is that it can be customized to fit the needs of different use cases. The encoder architecture can be any neural network which can be initialized with custom weights if needed. The aggregator can also be chosen arbitrarily. In our experiments we focus on the popular architecture gated MIL attention³, but any aggregation method can be used as long as it can be trained on a single GPU. Multi-GPU aggregators could also be supported in the future.

Below we include torch-like pseudocode that illustrates the key aspects of the proposed framework. The code will be available on [GitHub](#).

```
1. # Initialize GPU processes
2. # Initialize data loader and models
3. # Initialize DDP group for encoder model
4. DDPgroup = dist.new_group(ranks=[1, ..., N])
5. encoder_model = DDP(encoder_model, group=DDPgroup)
6. for epoch in range(E):
7.     for i, batch in enumerate(loader):
8.         # Note that each optimization step is done for one slide
9.         # Data loader and distributed sampler are in charge of feeding the right data to each process
10.
11.        # Forward pass on encoder
12.        if rank != 0:
13.            features = encoder(batch)
14.
15.        # Gather features
16.        with torch.no_grad():
17.            if rank == 0:
18.                dist.gather(features, allfeatures, dst=0, group=None)
19.
20.        # Forward/Backward pass on aggregator
21.        if rank == 0:
22.            # Record gradients on features
23.            allfeatures.requires_grad_()
24.            # Forward pass aggregator
25.            output = aggregator(allfeatures)
26.            aggregator_loss = criterion(output, label)
27.            # Backward pass aggregator
28.            aggregator_loss.backward()
29.            # Get feature gradients
30.            grads = allfeatures.grad.detach()
31.
32.        # Scatter feature gradients
33.        with torch.no_grad():
34.            dist.scatter(grads_recv, grads, src=0, group=None)
35.
36.        # Backward pass encoder
37.        # Generate loss on DDP group
38.        # Loss has to be scaled by number of DDP processes
39.        if rank != 0:
40.            encoder_loss = pseudo_loss(features, grads_recv) * (world_size-1)
41.            encoder_loss.backward()
```

Results

Gradient Equivalence

In this section we provide experimental evidence of the equivalence of single and multi-GPU runs by inspecting gradients in a simple deterministic toy network and in a non-deterministic convolutional neural network.

To determine the equivalence of the proposed GPU parallelization strategy, we compared a single GPU run of a toy deterministic network to a parallelized multi-GPU run. To ensure reproducibility between runs and across GPU processes, we manually set the random seed and used the following settings in torch which allow to run in a deterministic fashion: `torch.backends.cudnn.benchmark = False` and `torch.backends.cudnn.deterministic = True`. Both encoder and aggregator networks were composed of linear layers and ReLU non linearities. The input to both runs was a randomly generated 800 by 2,048 matrix. In the single GPU run the entire input was fed through the encoder and aggregator networks, while in the parallelized version the input was split across 4 GPUs and the

aggregation was done on a fifth GPU. Gradients for both networks were stored after loss computation for comparison. We were able to establish the equivalence of the gradients.

Neural networks used in practice are implemented in a non-deterministic way due to the nature of GPU computations. Here we test the framework using realistic encoders and aggregators, namely a ResNet50 and GMA. For this experiment we stored parameters and gradients of the first convolutional layer (Encoder Conv 1) and the first convolutional layer of the last block in the last layer of the encoder (Encoder Conv 51) as well as the classification layer in the aggregator (Classifier). Additionally, we also record the loss at each step. To maximize reproducibility, image augmentations were not performed, GMA was instantiated without dropout, and the batch normalization layers were synchronized. This is in contrast with running experiments in practice where we perform augmentations, use dropout, and do not synchronize the batch normalization layers. We measured the normalized L1 distance between parameter and gradient vector of the single GPU run and the multi-GPU run and followed these measurements for several optimization steps. In Figure 3 we show the results of this experiment. We can see that despite our efforts, differences in parameters, loss, and gradients can be observed. These differences have a small magnitude and seem to plateau after a few optimization steps. In practice this difference does not have a significant effect on training as we will show in the next section.

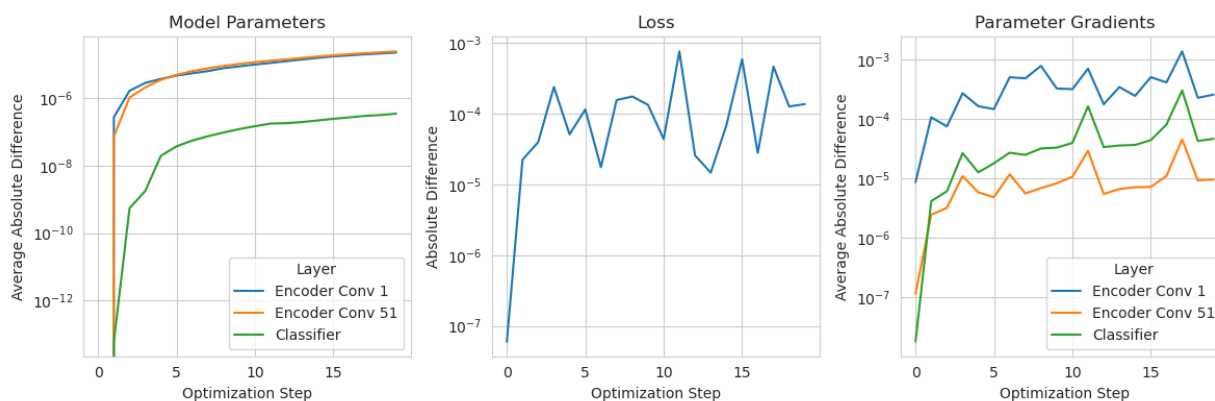


Figure 3. Gradient equivalence in real world networks. We tracked parameters and gradients of three layers in the network, including two convolutional layers from the encoder and the classification layer of the aggregator. Left) Normalized L1 norm of the difference between model parameters in single and multi-GPU experiments. Middle) Absolute difference in the loss between single and multi-GPU experiments. Right) Normalized L1 norm of the difference between model parameters' gradients in single and multi-GPU experiments.

Application to Real-World Data

Lung Adenocarcinoma EGFR Mutation Prediction

In this section we describe experiments performed on real-world clinical data where we applied the proposed method to the prediction of EGFR mutational using a large clinical dataset described in Campanella et al.¹⁷. The dataset consists of 2,449 digitized slides from 2,056 lung adenocarcinoma patients collected at MSKCC paired with EGFR mutational status derived from the IMPACT sequencing panel¹⁸. We used the same Monte Carlo Cross Validation scheme as in Campanella et al.¹⁷ where 1,951 slides were used for training and 498 for validation with 20 randomly generated splits. At each epoch, 50% of the slides were selected for training to speed up the experiments. For each slide, K tiles were sampled at random. If a slide contained less than K tiles, sampling with replacement was performed. Tiles were loaded on the fly using the `cucim` library from NVIDIA¹⁹, no pre-tiling of the slides was

performed. We trained a ResNet50 model using the proposed framework with increasing number of K tiles per slide from 50 to 4,900. With $K \in \{50, 100, 350, 700\}$ we used a single GPU, while with $K \in \{700, 2100, 4900\}$ we used our parallel implementation with up to 8 GPUs. For each value of K in the multi-GPU setting, we compared training with full precision and AMP. Experiments were run on a cluster of H100 GPUs.

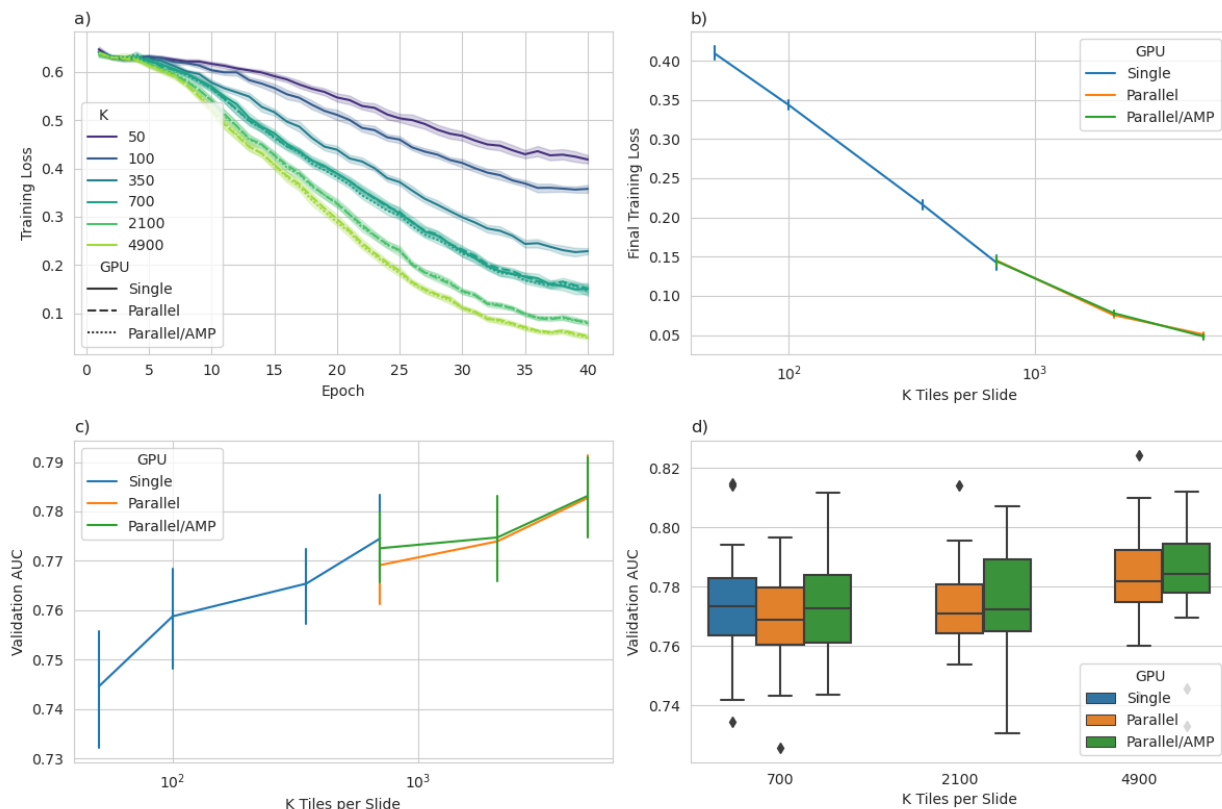


Figure 4. EGFR Mutation Prediction in LUAD Experiments. a) Training loss convergence curves stratified by K tiles per slide and GPU parallelization strategy. Each curve summarizes the 20 MCCV runs. The shaded area is calculated by bootstrapping with 95% confidence intervals (CI). b) Final Training loss stratified by GPU parallelization strategy in relation to K tiles per slide. Each point is the average over the 20 MCCV runs, and the error bar is estimated via bootstrapping using 95% CI. c) Validation AUC stratified by GPU parallelization strategy in relation to K tiles per slide. Each point is the average over the 20 MCCV runs, and the error bar is the 95% CI average estimate calculated via bootstrapping. d) Comparison of validation AUCs between GPU parallelization strategies. Each boxplot represents the distribution of validation AUCs of the 20 MCCV runs.

In Figure 4 we present the results of these experiments. It can be observed that the training loss decreases as K increases. Importantly, there is no significant difference in loss when comparing single and parallel runs (see $K=700$ in Figure 4a). This is an additional validation of the equivalence of these GPU strategies. Further, full precision and AMP runs are also comparable in terms of training loss. In Figure 4b we plotted the final training loss against K tiles and observed a log exponential decay of the loss as K increases. It is likely that a further decrease in loss could be observed for larger K values. In terms of validation AUC, we recorded the best validation AUC for each MCCV split. In Figure 4c we plot the validation AUC stratified by GPU parallelization strategy in relation to the values of K and observe that the estimate of average AUC increases with larger K values. It is possible that further increase of K may result in higher validation AUCs. Additionally, the different GPU strategies result in similar performance in terms of validation AUC. This is confirmed in Figure 4d where we show the full

distribution of validation AUC values for experiments where several GPU strategies were employed. In summary, we determined that increasing K results in lower training loss and higher validation AUC and confirmed that the various GPU strategies are equivalent. In Table 1 we compare these results with previous published and unpublished results on this same dataset using a variety of training strategies. These include: i) training in a supervised manner from all tissue tiles with slide-level targets as in Coudray et. al.²⁰, ii) training in a supervised manner only from tumor tiles, iii) using max-pool MIL as in Campanella et. al.², iv) training a GMA aggregator based on the supervised features learned in strategy ii, v) training a transMIL⁴ aggregator based on the supervised features learned in strategy ii, vi) training a GMA aggregator using an ImageNet pre-trained truncated ResNet50 as popularized by Lu et al.²¹, vii-viii) training a GMA aggregator using DINO trained ViT models described in Campanella et al.¹¹. Some of these strategies require significantly more effort and resources. Strategy iv for example requires training a tumor segmentation model, then training a tile encoder model on tumor tiles, and finally training a slide-aggregation model. Strategies vii and viii require access to hundreds of thousands of slides and thousands of GPU hours to train a SSL tile encoder before training a slide encoder. Yet, compared to previous strategies, the proposed method’s performance is on par or better while processing a relatively low number of tiles per slide. It is interesting to note that while it is possible to process an entire slide with enough GPUs, in many cases it may be enough to use a smaller value of K.

Algorithm	Embedding	Tiles	AUC Avg (Std)	Source
Supervised	NA	All Tiles	71.0 (4.7)	¹⁷
Supervised	NA	Tumor Tiles	74.6 (5.3)	¹⁷
Max-pool MIL ²	NA	All Tiles	68.0 (2.6)	Unpublished
GMA ³	Supervised Tumor	All Tiles	78.8 (2.8)	¹⁷
TransMIL ⁴	Supervised Tumor	All Tiles	73.9 (4.2)	¹⁷
GMA ³	tResNet50 ImageNet	All Tiles	64.9 (3.1)	¹¹
GMA ³	DINO ViT-small 423k	All Tiles	75.3 (3.0)	¹¹
GMA ³	DINO ViT-base 423k	All Tiles	76.6 (2.4)	Unpublished
Proposed				
K=50	NA	All Tiles	74.4 (2.9)	NA
K=100			75.9 (2.5)	
K=350			76.5 (1.7)	
K=700 (S)			77.5 (2.0)	
K=700 (P)			76.9 (2.9)	
K=700 (H)			77.3 (1.7)	
K=2100 (P)			77.4 (1.5)	
K=2100 (H)			77.5 (2.1)	
K=4900 (P)			78.3 (1.9)	
K=4900 (H)			78.3 (1.9)	

Table 1. Comparison of performance on the EGFR prediction task of popular training strategies from published and unpublished results. For the proposed method, we show the results for various values of K and GPU parallelization strategies. S stands for single GPU, P stands for parallel GPUs, H stands for parallel GPUs with half precision.

Breast Cancer Detection

In this section we describe how we applied the proposed system to a cancer detection task and trained a model end-to-end on the entire slide at 20x magnification. From our institution’s research slide archive we queried all scanned and de-identified H&E breast slides from the beginning of the scanning initiative

until September 2023. On these cases, we automatically extracted cancer status (benign vs cancer) at the specimen level from the pathology laboratory information systems (LIS). We were able to obtain an automatically curated dataset of 77,768 slides, where 67,654 were negative and 10,114 were positive. We further sampled this cohort to obtain a balanced dataset of 16,302 slides. The data was then divided at the patient level in a training split consisting of 13,050 slides and a validation split consisting of 3,252 slides. We calculated the maximum number of tissue tiles of size 224 pixels per slide on this cohort. To allow for full slide analysis, we parallelized encoding with a ResNet18 network on 11 GPUs with K=4,096 tiles per GPU, enabling training up to 45,056 tiles per slide. We trained the encoder and a GMA aggregator jointly, end-to-end on 12 H100 80GB GPUs. At each epoch, 50% of the slides were sampled for training. We used the AdamW²² optimizer and a peak learning rate of 0.00005 based on previous experiments. No hyperparameter tuning was performed. In Figure 5 we show training and validation results of this experiment. We found a maximum validation AUC of 0.968 after 30 epochs, after which we can see signs of overfitting.

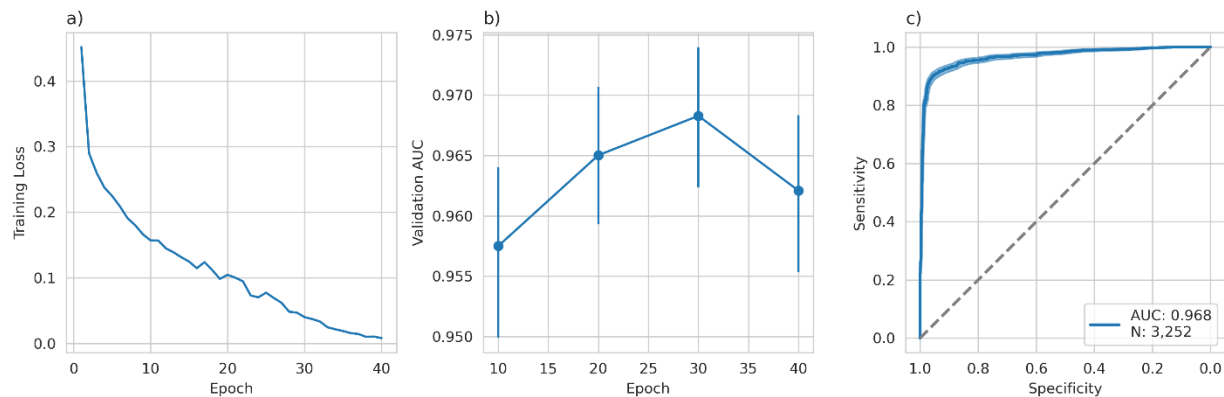


Figure 5. Breast Cancer Detection Experiment. a) Training loss convergence. b) Validation AUC convergence. c) ROC curve for the best validation result.

Discussion

Recent advances in computer vision and computational pathology, along with the digitization of pathology data, have enabled the development of decision support systems tailored to a wide variety of clinical tasks, from quality control to survival analysis. Despite the numerous efforts in this space, so far only one system has found its way into clinical practice²³. While diagnostic decision support systems in pathology have met the high standards of clinical application, the same is not true for many other tasks where computational pathology may be of great benefit. These include biomarker prediction, treatment response prediction, and treatment recommendation. While in diagnostic tasks, the signal is generally well defined and recognizable by human experts and is contained within small tissue regions, for other more complex tasks the source of the signal, if at all present, is largely unknown. It is possible that local and global spatial arrangements of cells may be informative and methods that can capture both may be more suited for some tasks such as outcome prediction. Current methods in computational pathology rely on a two-step approach where features are independently learned at a tile-level, and then aggregated at a slide-level. This has proven successful for some tasks, especially cancer detection and classification, but it has not seen the same level of success in many other tasks.

By connecting both steps in an end-to-end fashion, it may be possible to obtain a better representation of a pathology slide which could yield better results for certain tasks, and research in this direction is starting to appear. In this work we present a framework that allows for the analysis of an entire pathology slide. Unlike Wang et. al.¹⁴, our framework relies on full resolution slides and is modular, allowing encoders and aggregators to be chosen to fit the needs and resources of a particular project. In addition, their resizing strategy may be problematic since it can introduce large variations in pixel resolution. This may not be as problematic in TCGA slides, but in real life samples, slide dimensions can vary widely depending on the amount of tissue on the slide.

Our proposed strategy parallelizes encoding to multiple GPUs and uses customized GPU communications to connect gradients from the slide-level aggregator back to the encoder. This workflow is mathematically equivalent to a single GPU run as we have shown in the gradient equivalence experiments. We applied our framework to the clinically relevant task of predicting EGFR mutations in lung adenocarcinoma patients. We showed that our single step approach is superior to all previous training strategies including large-scale SSL pre-training.

While the proposed method can be scaled up to analyze an entire slide end-to-end, it is also amenable to more modest set-ups by simply sampling fewer tiles per slide. In our experiments we have shown that this strategy can be effective. Our proposed method can be trained from scratch on a specific task, or finetuned from a pre-trained encoder. Yet, we argue that the best use of this framework will be in the training of pathology foundation models based on large-scale clinical datasets. This work opens the possibility to train better encoders based on slide-level targets. Current strategies rely on applying SSL algorithms to tiles extracted from pathology slides. While these SSL trained encoders are an improvement over natural images pre-trained networks, we expect further improvements by directly supervising training on pathology relevant tasks. In future experiments we plan to use the proposed framework to train a large foundation model based on slide-level signals automatically extracted from the pathology LIS.

References

1. Dietterich, T. G., Lathrop, R. H. & Lozano-Pérez, T. Solving the multiple instance problem with axis-parallel rectangles. *Artif. Intell.* **89**, 31–71 (1997).
2. Campanella, G. *et al.* Clinical-grade computational pathology using weakly supervised deep learning on whole slide images. *Nat. Med.* **25**, 1301–1309 (2019).
3. Ilse, M., Tomczak, J. M. & Welling, M. Attention-based Deep Multiple Instance Learning. (2018) doi:10.48550/ARXIV.1802.04712.
4. Shao, Z. *et al.* TransMIL: Transformer based Correlated Multiple Instance Learning for Whole Slide Image Classification. (2021) doi:10.48550/ARXIV.2106.00908.

5. Kang, M., Song, H., Park, S., Yoo, D. & Pereira, S. Benchmarking Self-Supervised Learning on Diverse Pathology Datasets. (2022) doi:10.48550/ARXIV.2212.04690.
6. Wang, X. *et al.* Transformer-based unsupervised contrastive learning for histopathological image classification. *Med. Image Anal.* **81**, 102559 (2022).
7. Filiot, A. *et al.* *Scaling Self-Supervised Learning for Histopathology with Masked Image Modeling.* <http://medrxiv.org/lookup/doi/10.1101/2023.07.21.23292757> (2023)
doi:10.1101/2023.07.21.23292757.
8. Chen, R. J. *et al.* Scaling Vision Transformers to Gigapixel Images via Hierarchical Self-Supervised Learning. (2022) doi:10.48550/ARXIV.2206.02647.
9. Chen, R. J. *et al.* A General-Purpose Self-Supervised Model for Computational Pathology. (2023)
doi:10.48550/ARXIV.2308.15474.
10. Vorontsov, E. *et al.* Virchow: A Million-Slide Digital Pathology Foundation Model. (2023)
doi:10.48550/ARXIV.2309.07778.
11. Campanella, G. *et al.* Computational Pathology at Health System Scale -- Self-Supervised Foundation Models from Three Billion Images. (2023) doi:10.48550/ARXIV.2310.07033.
12. Xie, C. *et al.* Beyond Classification: Whole Slide Tissue Histopathology Analysis By End-To-End Part Learning. in *Proceedings of the Third Conference on Medical Imaging with Deep Learning* (eds. Arbel, T. *et al.*) vol. 121 843–856 (PMLR, 2020).
13. Qu, L., Luo, X., Wang, M. & Song, Z. Bi-directional Weakly Supervised Knowledge Distillation for Whole Slide Image Classification. (2022) doi:10.48550/ARXIV.2210.03664.
14. Wang, W. *et al.* When an Image is Worth 1,024 x 1,024 Words: A Case Study in Computational Pathology. Preprint at <http://arxiv.org/abs/2312.03558> (2023).
15. Ding, J. *et al.* LongNet: Scaling Transformers to 1,000,000,000 Tokens. Preprint at <http://arxiv.org/abs/2307.02486> (2023).

16. Li, S. *et al.* PyTorch Distributed: Experiences on Accelerating Data Parallel Training. (2020)
doi:10.48550/ARXIV.2006.15704.
17. Campanella, G. *et al.* H&E-based Computational Biomarker Enables Universal EGFR Screening for Lung Adenocarcinoma. *ArXiv Prepr. ArXiv220610573* (2022).
18. Cheng, D. T. *et al.* Comprehensive detection of germline variants by MSK-IMPACT, a clinical diagnostic platform for solid tumor molecular oncology and concurrent cancer predisposition testing. *BMC Med. Genomics* **10**, 33 (2017).
19. cuCIM. RAPIDS (2023).
20. Coudray, N. *et al.* Classification and mutation prediction from non–small cell lung cancer histopathology images using deep learning. *Nat. Med.* **24**, 1559–1567 (2018).
21. Lu, M. Y. *et al.* Data-efficient and weakly supervised computational pathology on whole-slide images. *Nat. Biomed. Eng.* **5**, 555–570 (2021).
22. Loshchilov, I. & Hutter, F. Decoupled Weight Decay Regularization. (2017)
doi:10.48550/ARXIV.1711.05101.
23. Commissioner, O. of the. FDA Authorizes Software that Can Help Identify Prostate Cancer. *FDA*
<https://www.fda.gov/news-events/press-announcements/fda-authorizes-software-can-help-identify-prostate-cancer> (2021).